DOI: 10.1002/chem.200600094

Heterocyclic Quinol-Type Fluorophores: Synthesis, X-ray Crystal Structures, and Solid-State Photophysical Properties of Novel 5-Hydroxy-5-substituent-benzo[*b*]naphtho[1,2-*d*]furan-6-one and 3-Hydroxy-3-substituent-benzo[*kl*]xanthen-2-one Derivatives**

Yousuke Ooyama, Tomohiro Okamoto, Takahiro Yamaguchi, Toshihisa Suzuki, Akiko Hayashi, and Katsuhira Yoshida*[a]

Abstract: Novel heterocyclic quinol-type fluorophores (**4a–c**) and (**5a–c**) that contain substituents (R = Me, Bu, Ph) with nonconjugated linkages to the chromophore skeleton have been synthesized and their photophysical properties have been investigated in solution and in the solid state. Considerable differences in the absorption and fluorescence spectra were observed between the two states. Quinols **4a–c** and **5a–c** exhibited almost the same absorption and fluorescence spectra in solution; however, their solid-state fluorescence excitation and emission spectra in the crystalline state were quite different. We performed X-ray crystallographic analyses to elucidate the dramatic effect of the substituents of the nonconjugated linkage on the solid-state fluorescence excitation and emission spectra. The relationships between the solid-state photophysical properties and the chemical and crystal structures of **4a–c** and **5a–c** are discussed on the basis of the X-ray crystal structures.

Keywords: crystal structures · dyes/pigments · fluorescence · heterocycles · substituent effects

Introduction

Organic fluorophores exhibiting strong solid-state emission properties have attracted increasing interest because of their many uses in the fundamental research field of solid-state photochemistry[1] and in the applied field of optoelectronic devices.[2] Although there are many dyes exhibiting strong fluorescence in solution, the number of fluorescent dyes exhibiting intense fluorescence in the solid state is relatively limited because most organic fluorophores undergo fluorescence quenching in the aggregation state. Much research has focused on the development of new strong solid-emissive fluorophores. For example, the introduction of bulky substituents onto the original fluorophores,[1c,f,2j,f,3] and the formation of clathrates[4,5] or salts[1h] with fluorophores are known to be useful methods to solve the problem of fluorescence quenching by aggregation. The correlation between the solid-state fluorescence properties and the molecular packing structures on the basis of the X-ray crystal structures have also been investigated to elucidate the details of fluorescence quenching.[1e–g,3,5–8] A strong intermolecular π–π interaction[1e–g,3,5,7] or continuous intermolecular hydrogen bonding[3b,6] between neighboring fluorophores have been postulated as being main contributors to fluorescence quenching. Ultimately, the key factor in the design of new, strong, solid-state emissive fluorophores is to eliminate parameters that induce concentration quenching in molecular aggregation states.

We have used a series of heterocyclic quinol-type fluorophores to demonstrate that the intermolecular π–π interactions of fluorophores have a decisive influence on the solid-state fluorescence properties.[3,5] We also discovered that quinol-type fluorophores exhibit significant changes of color and a drastic fluorescence enhancement upon inclusion of guest molecules in the crystalline state. The relationship between the solid-state fluorescence properties and the crystal structures confirms that the destruction of π–π interactions between the fluorophores by guest enclathration is the main reason for the guest-dependent fluorescence enhancement

[a] Dr. Y. Ooyama, T. Okamoto, T. Yamaguchi, T. Suzuki, A. Hayashi, Prof. Dr. K. Yoshida
Department of Material Science, Faculty of Science
Kochi University
Akebono-cho, Kochi 780–8520 (Japan)
Fax: (+81) 88-844-8359
E-mail: kyoshida@cc.kochi-u.ac.jp

[**] Heterocyclic Quinol-type Fluorophores, Part 5; for Part 4, see: Y. Ooyama, K. Yoshida, *New J. Chem.* **2005**, *29*, 1204.

Pagination corrected Oct. 17, 2006

behavior. Herein, we report on new heterocyclic quinol-type fluorophores, 5-hydroxy-5-substituent-benzo[*b*]naphtho[1,2-*d*]furan-6-one (**4**) and 3-hydroxy-3-substituent-benzo[*kl*]-xanthen-2-one (**5**) fluorophores, whose solid-state fluorescence can be dramatically changed by introduction of substituents on the nonconjugated linkage to the quinol skeleton. We carried out X-ray crystallographic analyses of **4a–c** and **5a–c** to elucidate the relationship between the photophysical properties and the chemical and crystal structures.

Results and Discussion

Synthesis of 5-hydroxy-5-substituent-benzo[*b*]naphtho[1,2-*d*]furan-6-one (4a–c) and 3-hydroxy-3-substituent-benzo[*kl*]xanthen-2-one (5a–c) fluorophores: We first prepared the starting heterocyclic quinones **2** and **3**. As shown in Scheme 1 and Table 1, selective synthesis of **1** and **2** was achieved by changing the solvent. When DMSO or DMF was used, quinone **1** was preferentially obtained (Table 1, runs 1, 2, 4, 5, 7, and 8). Whereas, when acetic acid was used, quinone **2** was preferentially obtained (Table 1, runs 3, 6, and 9). The reaction was efficiently promoted by an addition of a metal salt, such as $NiCl_2$ or $CuCl_2$ (Table 1, runs 4–9). The formation of a metal chelate complex between the *o*-quinone carbonyl groups and the metal ion probably facilitates the nucleophilic desulfoarylation at the 4-position.[9] We also found that not only quinone **2** but also quinone **3** are selectively obtained by heating quinone **1** in various solvents in the presence of a metal salt (Scheme 1, Table 2). The intramolecular cyclization reaction barely proceeded in DMSO or DMF in the absence of a metal salt (Table 2,

Table 1. Effects of metal salt and solvent on the reaction of sodium 1,2-naphthoquinone-4-sulfonate with *m*-dibutylaminophenol.[a]

Run	Metal salt	Solvent	Time [h]	Product yield [%]	
				1	**2**
1	none	DMF	10	22	1.8
2	none	DMSO	10	10	2.1
3	none	CH_3COOH	15	1.0	8.4
4	$NiCl_2$	DMF	5	37	1.1
5	$NiCl_2$	DMSO	5	15	2.4
6	$NiCl_2$	CH_3COOH	8	1.5	38
7	$CuCl_2$	DMF	5	32	1.1
8	$CuCl_2$	DMSO	5	12	1.8
9	$CuCl_2$	CH_3COOH	7	1.2	42

[a] Sodium 1,2-naphthoquinone-4-sulfonate (3.84 mmol) was stirred with *m*-dibutylaminophenol (5.76 mmol) in various solvents (25 mL) in the absence or presence of a metal chloride (3.84 mmol) at 50 °C.

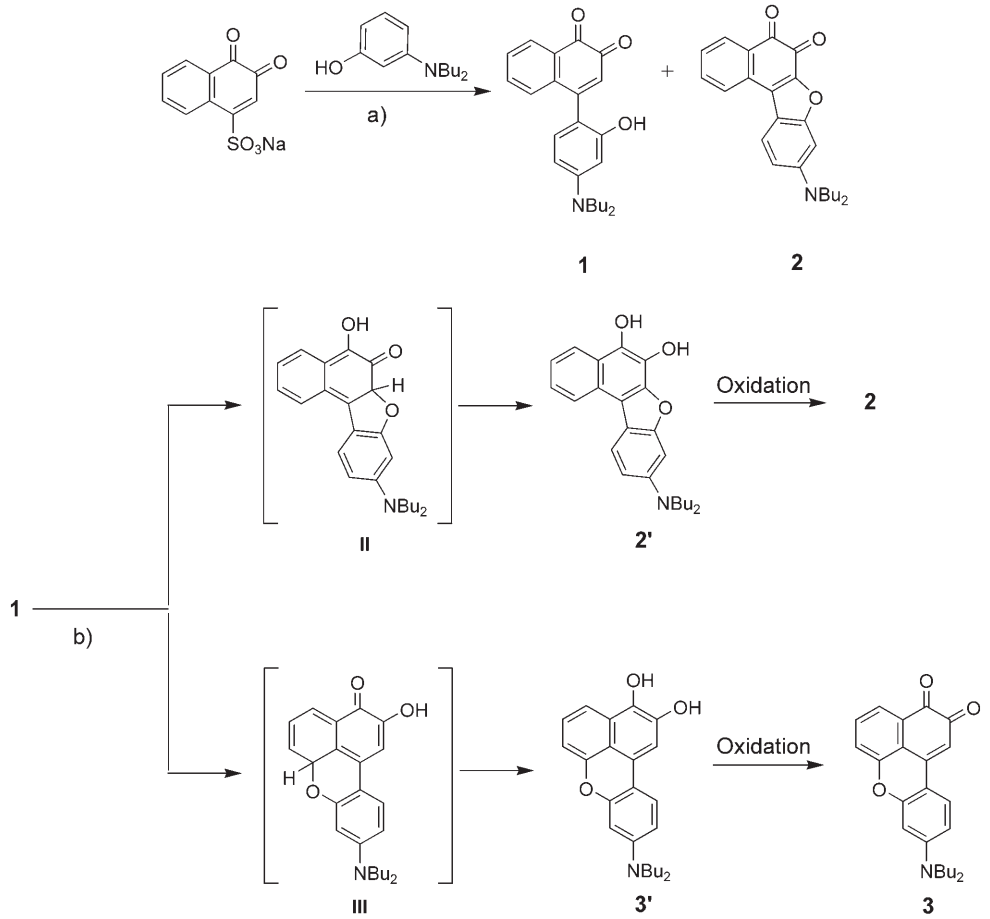

Scheme 1. Synthesis of *o*-quinones **1**, **2**, and **3**. a) Metal salt ($NiCl_2$ or $CuCl_2$), solvent (DMSO, DMF, or CH_3COOH), 50 °C, 5–10 h; b) metal salt ([Ni($OCOCH_3$)$_2$] or [Cu($OCOCH_3$)$_2$]), solvent (DMSO, DMF, CH_3COOH, 1,4-dioxane, or *N*-methyl-2-pyrrolydone), 100 °C, 3–72 h.

Table 2. Effects of metal salt and solvent on the intramolecular cyclization of the quinone **1**.[a]

Run	Metal salt	Solvent	Time [h]	Product yield [%]	
				2	**3**
1	none	DMF	72	0.9	1.0
2	none	DMSO	72	1.2	0.8
3	none	CH_3COOH	72	17	14
4	$[Ni(OCOCH_3)_2]$	DMF	16	37	23
5	$[Ni(OCOCH_3)_2]$	DMSO	12	21	58
6	$[Ni(OCOCH_3)_2]$	CH_3COOH	13	19	15
7	$[Cu(OCOCH_3)_2]$	1,4-dioxane	15	41	26
8	$[Cu(OCOCH_3)_2]$	NMP[b]	5	35	39
9	$[Cu(OCOCH_3)_2]$	DMF	7	41	26
10	$[Cu(OCOCH_3)_2]$	DMSO	7	15	66
11	$[Cu(OCOCH_3)_2]$	CH_3NO_2	3	80	0
12	$[Cu(OCOCH_3)_2]$	CH_3COOH	7	19	18

[a] Quinone **1** (3.84 mmol) was stirred in various solvents (25 mL) in the absence or presence of metal acetate (3.84 mmol) at 100 °C. [b] *N*-methyl-2-pyrrolidone.

runs 1 and 2). However, the reaction proceeded slowly in acetic acid to give **2** and **3** in 17% and 14% yields, respectively (Table 2, run 3). Apparently, the reaction was efficiently promoted by the addition of $[Ni(OCOCH_3)_2]$ or $[Cu(OCOCH_3)_2]$ in various solvents to give quinones **2** and **3** in moderate yields (Table 2, runs 4–12). The activity of the metal acetates was in the order $Cu^{II} > Ni^{II}$; the oxidative Cu^{II} ion would work more effectively for the completion of the intramolecular cyclization. We also discovered that the product ratio (**2** vs. **3**) of the intramolecular cyclization reaction was greatly dependent on the nature of the solvent used (Table 2, runs 7–12). The reaction in DMSO preferentially afforded quinone **3** (Table 2, run 10), whereas the preferential product from the reaction in nitromethane was quinone **2** (Table 2, run 11). A possible reaction pathway for the formation of **2** and **3** is shown in Scheme 2. The solvent effects on the regioselectivity of the intramolecular cyclization may be rationalized by the difference in the stabilization of the transition states (**II** and **III**; see Scheme 1) by solvation. The initial intramolecular cyclization of **1** to give hydroquinones **2′** and **3′**, and the subsequent oxidation to **2** and **3** were efficiently promoted by adding $[Cu(OCOCH_3)_2]$.

As shown in Scheme 2, quinols **4a–c** and **5a–c** were obtained by reacting quinones **2** and **3** with organolithium reagents (RLi: MeLi, BuLi, and PhLi) at −108 °C, respectively. It is known that the addition of organometallic reagents to quinones affords not only quinols, but also hydroquinone as a by-product: both the 1,2-addition and the reduction of the quinoid skeleton by organometallic reagents proceed competitively.[10] In our case, the corresponding hydroquinone produced in situ was easily reoxidized by atmospheric oxygen during workup of the reaction mixture, resulting in recovery of the starting quinone. For quinone **2**, the organolithium reagents preferentially attack the 5-carbonyl carbon rather than the 6-carbonyl carbon, in spite of the similar steric reactivity of the two carbonyl groups (Table 3). The conjugated linkage of the dibutylamino group to the 6-carbonyl group would make the 6-carbonyl carbon atom more weakly electrophilic than the 5-carbonyl carbon atom, so

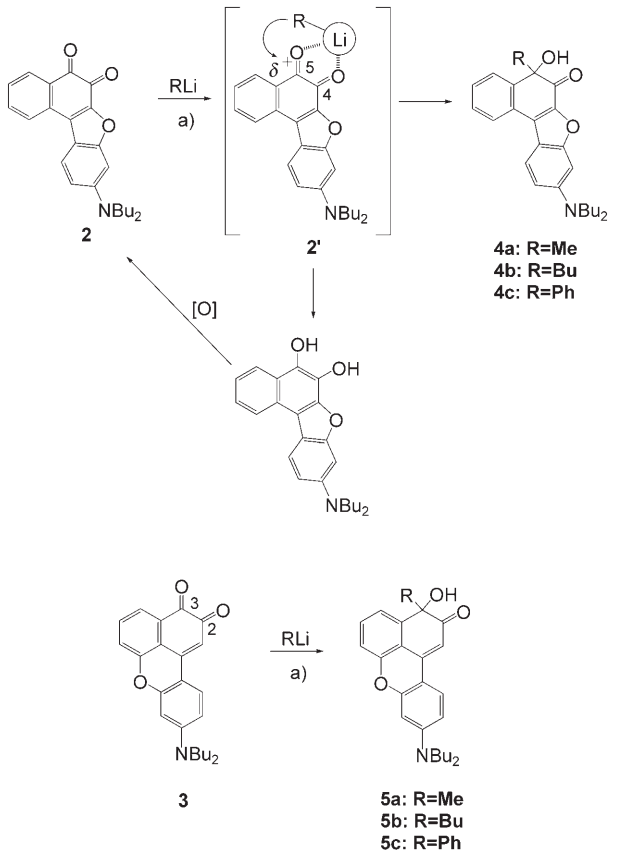

Scheme 2. Synthesis of quinols **4** and **5**. a) THF, −108 °C to RT, 30 min.

Table 3. Synthesis of the quinol by reaction of quinone with organolithium (RLi) reagents at −108 °C.

Run	RLi	Product		Recovered quinone [%]	
		Quinol	Yield [%]		
1	MeLi	**4a**	67	**2**	17
2	BuLi	**4b**	47	**2**	24
3	PhLi	**4c**	30	**2**	45
4	MeLi	**5a**	49	**3**	30
5	BuLi	**5b**	37	**3**	32
6	PhLi	**5c**	17	**3**	48

that the counteranions (R^-) preferentially attack the electrophilic 5-carbonyl carbon atom. The yield of the quinols was in the order **4a** > **4b** > **4c**, while the yield of recovered starting quinone **2** was in the reverse order. The reaction of quinone **3** with organolithium reagents can be explained similarly.

Spectroscopic properties of 4a–c and 5a–c in solution: The visible absorption and fluorescence spectral data of **4a–c** and **5a–c** in solution are summarized in Table 4. The fluorescence spectra of the quinols were recorded by excitation at the wavelengths of the absorption maximum with the longest wavelength. Owing to the nonconjugated linkage of the substituents (R = Me, Bu, and Ph) to the chromophore

Table 4. Absorption and fluorescence spectral data of **4a–c** and **5a–c** in solution.

Quinol	Solvent	Absorption λ_{max} [nm] (ε_{max} [dm^{3}mol^{-1}cm^{-1}])	Fluorescence λ_{max} [nm]	Φ	SS[a] $\Delta\lambda_{max}$ [nm]
4a	benzene	427 (22500)	470	0.76	43
	1,4-dioxane	421 (21300)	476	0.74	55
	THF	419 (20900)	494	0.60	75
	DMF	426 (20200)	524	0.35	98
	DMSO	430 (20400)	528	0.31	98
	acetonitrile	428 (20500)	524	0.30	96
	ethanol	432 (20400)	538	0.16	106
4b	1,4-dioxane	420 (21700)	476	0.74	56
	acetonitrile	430 (22600)	525	0.31	95
4c	1,4-dioxane	430 (21600)	484	0.74	55
	acetonitrile	441 (22400)	536	0.30	95
5a	cyclohexane	430(30200), 408(32500)	441	0.03	11
	diethyl ether	430(28400), 411(31300)	457	0.04	27
	1,4-dioxane	433(29400), 416(28200)	464	0.04	31
	THF	433(29700), 419(31100)	479	0.14	46
	DMF	438(29200)	503	0.27	65
	DMSO	441(28700)	506	0.27	65
	acetonitrile	438(32600)	501	0.46	63
	ethanol	442(33200)	508	0.33	66
5b	1,4-dioxane	434(29000), 417(28000)	465	0.04	31
	acetonitrile	440(32400)	501	0.43	61
5c	1,4-dioxane	442(31200), 426(30700)	472	0.03	30
	acetonitrile	450(35300)	507	0.43	57

[a] Stokes shift value.

skeleton, the absorption and fluorescence spectra of fluorophores **4a–c** or **5a–c** are very similar in each category.

Quinols **4a–c** exhibit an intense absorption band at about 420–430 nm and an intense fluorescence band at about 475–485 nm (Φ = 0.74–0.77) in 1,4-dioxane. The solvent effect was investigated with quinol **4a**, which showed that the fluorescence properties are significantly dependent on the solvent polarity. The absorption maximum of **4a** shows a small bathochromic shift of 5 nm from benzene to ethanol, while the fluorescence maximum shows a large bathochromic shift of 63 nm, so that the Stokes shift value in polar solvents becomes larger than that in nonpolar solvents. The fluorescence quantum yield (Φ) of **4a** is reduced to about 22% by changing the solvent from benzene to ethanol. Similar spectral changes were generally observed for most fluorescent dyes whose dipole moments in the excited state are larger than those in the ground state.

On the other hand, solvent effects on the absorption and fluorescence spectra of **5a–c** are quite different from those of **4a–c**. Quinol **5a** exhibits an intense absorption band at about 410–440 nm and a weak fluorescence band at about 440–480 nm (Φ = 0.03–0.14) in nonpolar solvents. However, in polar solvents, **5a** exhibits an intense absorption band at about 438–442 nm and an intense fluorescence band at about 501–508 nm (Φ = 0.27–0.46). The absorption maximum with the longest wavelength of **5a** shows a small bathochromic shift of 9 nm from 1,4-dioxane to ethanol, while the fluorescence maximum shows a large bathochromic shift of 44 nm, so that the Stokes shift value in polar solvents becomes larger than that in nonpolar solvents. As shown above, significant dependence of the fluorescence quantum yield (Φ) on the solvent polarity was also observed: the Φ value of **5a** is increased by a factor of 8 on changing the solvent from 1,4-dioxane to ethanol. Similar fluorescence characteristics were previously reported in some aromatic carbonyl compounds such as pyrene-3-carboxaldehyde,[11] 7-alkoxycoumarins,[12] and *o*-aminoacetophenone.[13]

Spectroscopic properties of 4a–c and 5a–c in the solid state: Interesting results have been obtained from the photophysical properties of crystalline **4a–c** and **5a–c**. Figure 1 shows that the optical properties of quinols **4a–c** and **5a–c** are quite different between the solution and the solid state. Crystals of **4c** exhibit strong greenish-yellow fluorescence emission, but the crystals of **4a** and **4b** exhibit yellowish-orange and green fluorescence emission, respectively. On the other hand, **5b** exhibits a strong green emission, whereas **5a** and **5c** exhibit relatively weak yellowish-orange and red emissions, respectively. In order to investigate the difference in the solid-state photophysical properties among **4a–c** or **5a–c**, we measured the fluorescence excitation and emission spectra of the crystals. As shown in Figure 2, quinol **4c** exhibits a stronger fluorescence band than the other quinols in the crystalline state: the fluorescence intensities of **4c** and **4b** are about 2.0-fold and 1.2-fold larger than that of **4a**, respectively. The wavelengths of the emission maximum of **4a** (λ_{em} = 560 nm), **4b** (λ_{em} = 530 nm), and **4c** (λ_{em} = 555 nm)

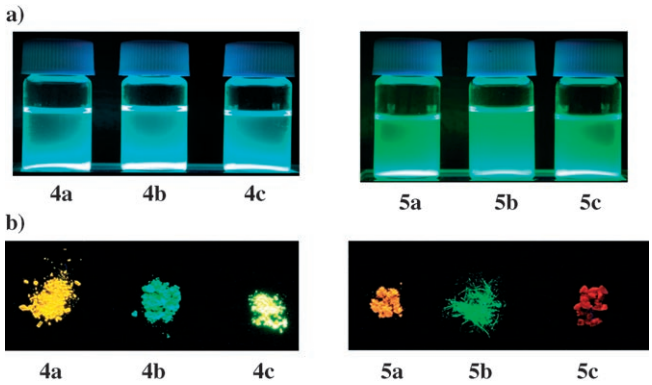

Figure 1. Fluorescence properties of **4a–c** and **5a–c:** a) in solution (1,4-dioxane for **4a–c** and DMSO for **5a–c**), and b) in the solid state.

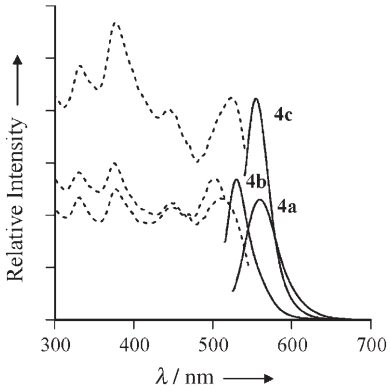

Figure 2. Solid-state excitation (-----) and emission (——) spectra of the crystals of **4a–c**: **4a**: $\lambda_{ex} = 510$ nm, $\lambda_{em} = 560$ nm; **4b**: $\lambda_{ex} = 503$ nm, $\lambda_{em} = 530$ nm; **4c**: $\lambda_{ex} = 519$ nm, $\lambda_{em} = 555$ nm.

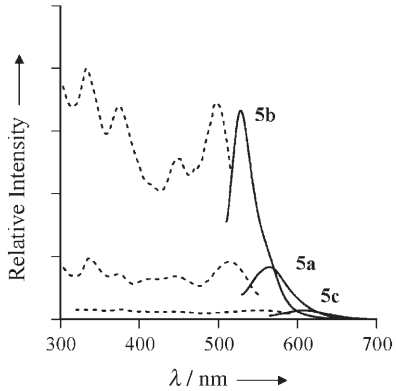

Figure 3. Solid-state excitation (-----) and emission (——) spectra of the crystals of **5a–c**: **5a**: $\lambda_{ex} = 514$ nm, $\lambda_{em} = 564$ nm; **5b**: $\lambda_{ex} = 497$ nm, $\lambda_{em} = 529$ nm; **5c**: $\lambda_{ex} = 550$ nm, $\lambda_{em} = 608$ nm.

are red-shifted by 84, 54, and 70 nm, respectively, compared to that in 1,4-dioxane.

On the other hand, quinol **5b** exhibits a much stronger fluorescence intensity than quinols **5a** and **5c** in the crystalline state (Figure 3). The fluorescence intensity of **5b** is about 8-fold and 32-fold larger than those of **5a** and **5c** in the solid state, respectively. The longest wavelengths of the excitation and the emission maxima of **5b** ($\lambda_{ex} = 497$ nm, $\lambda_{em} = 529$ nm) in the crystalline state are red-shifted by 63 and 64 nm, respectively, compared with those of the absorption and the emission maxima of **5b** in 1,4-dioxane. In contrast, the longest wavelengths of the excitation and the emission maxima of **5c** ($\lambda_{ex} = 550$ nm, $\lambda_{em} = 608$ nm) in the crystalline state have large red shifts of 108 and 136 nm, respectively, with respect to those of the absorption and the emission maxima of **5c** in 1,4-dioxane.

X-ray crystal structures of 4a–c and 5a–c: To understand the dramatic substituent effect on the solid-state photophysical properties, the X-ray crystal structures of quinols **4a–c** and **5a–c** were determined and are shown in Figures 4–9, respectively. The crystal systems of **4a–c** and **5a–c** are summarized in Tables 5 and 6. The packing structures demonstrate that the quinol molecules of **4a–c** are arranged in a "bricks in a wall" fashion. The crystals of **4a–c** are built up of a centrosymmetric dimer unit that is composed of a pair of quinol enantiomers. In the crystals of **4a** and **4c**, neighboring enantiomers are connected by two intermolecular hy-

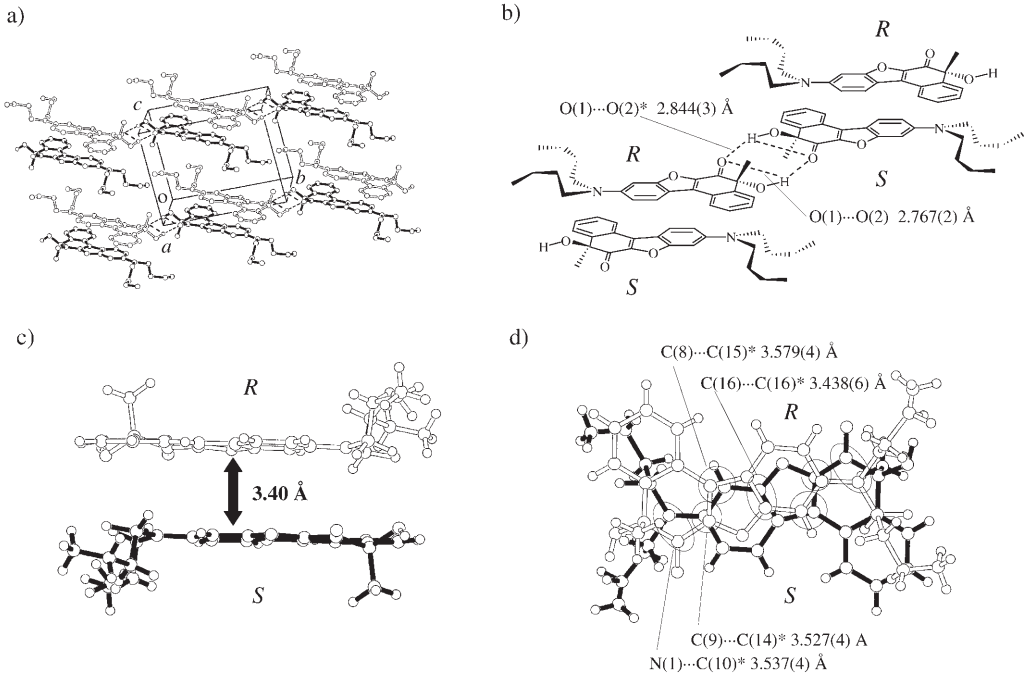

Figure 4. Crystal packing and hydrogen-bonding pattern of **4a**: a) stereoview of the molecular packing structure, b) schematic structure, c) side view, and d) top view of the pairs of fluorophores.

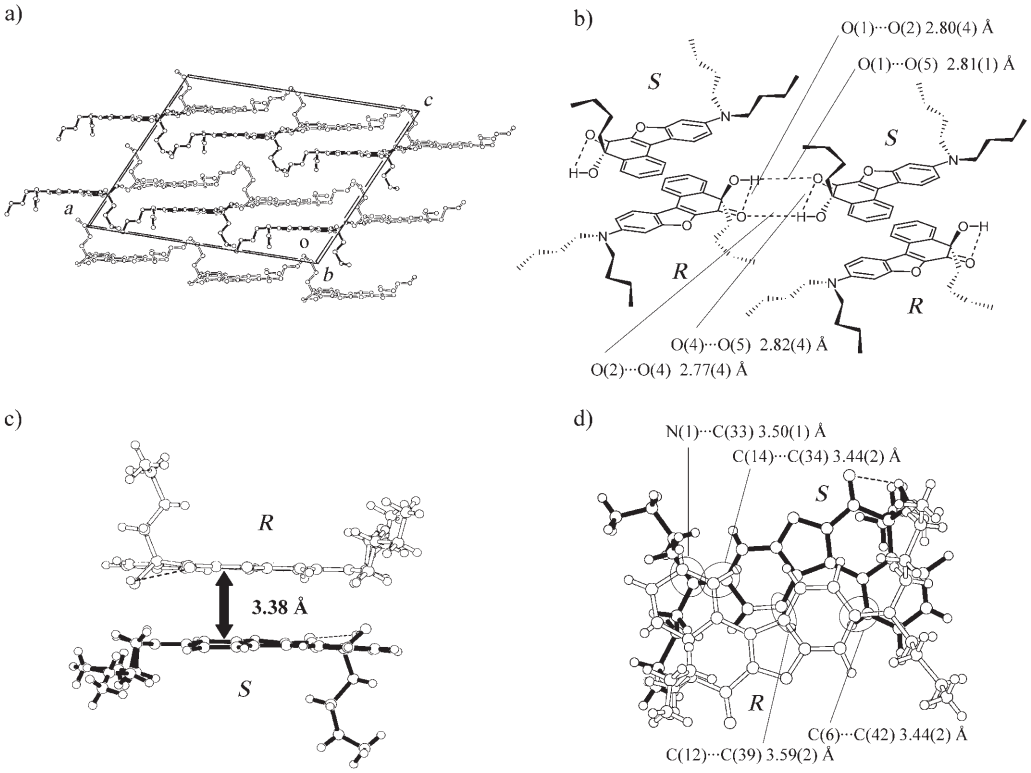

Figure 5. Crystal packing and hydrogen-bonding pattern of **4b**: a) stereoview of the molecular packing structure, b) schematic structure, c) side view, and d) top view of the pairs of fluorophores.

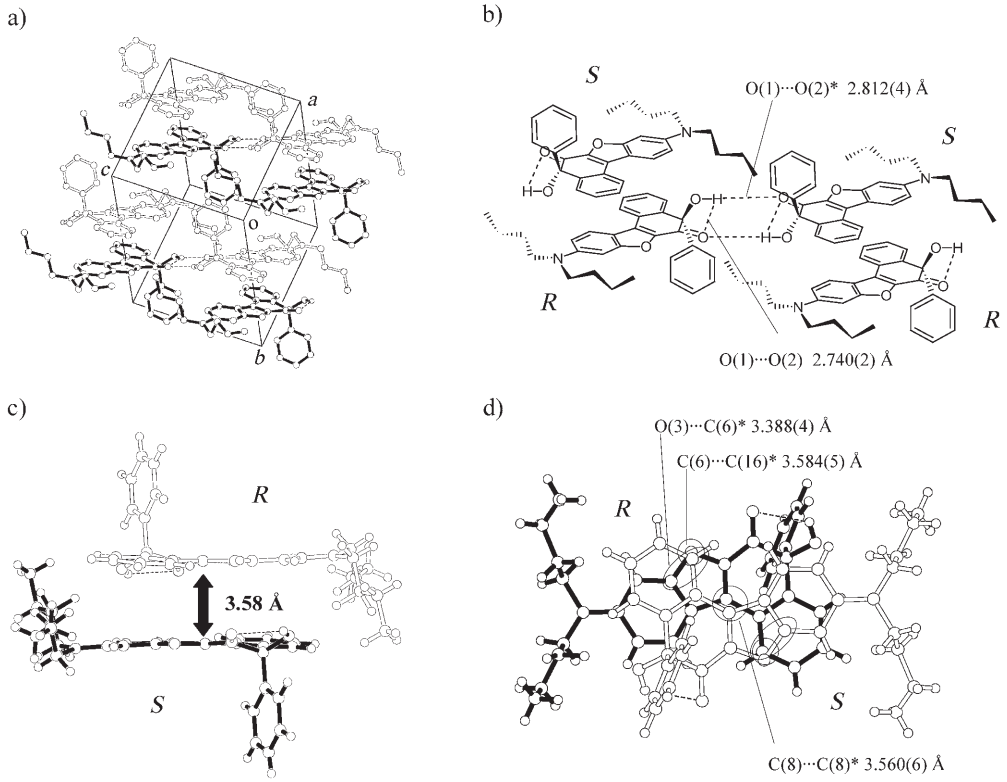

Figure 6. Crystal packing and hydrogen-bonding pattern of **4c**: a) stereoview of the molecular packing structure, b) schematic structure, c) side view, and d) top view of the pairs of fluorophores.

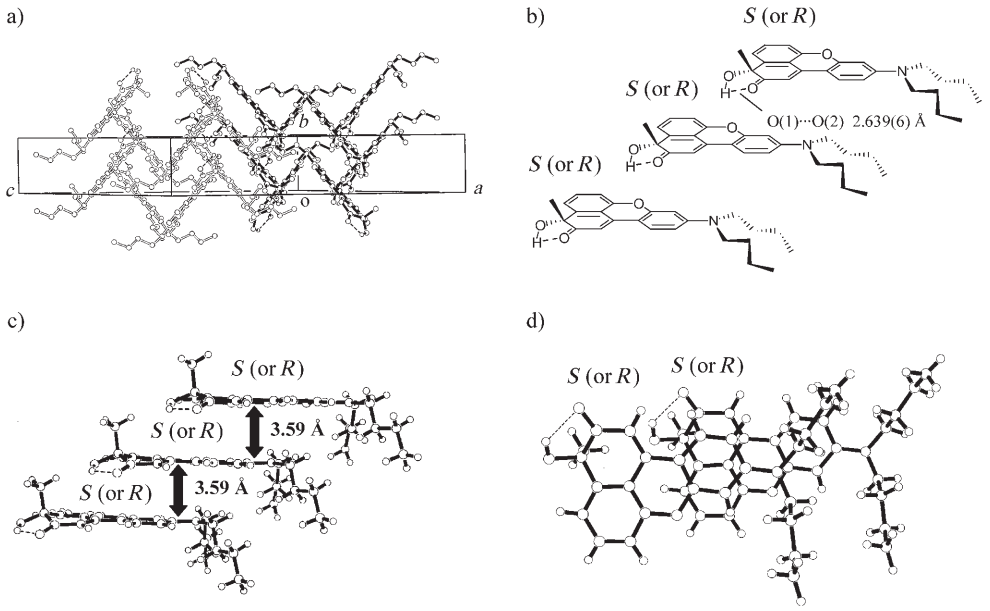

Figure 7. Crystal packing and hydrogen-bonding pattern of **5a**: a) stereoview of the molecular packing structure, b) schematic structure, c) side view, and d) top view of the overlapping of fluorophores.

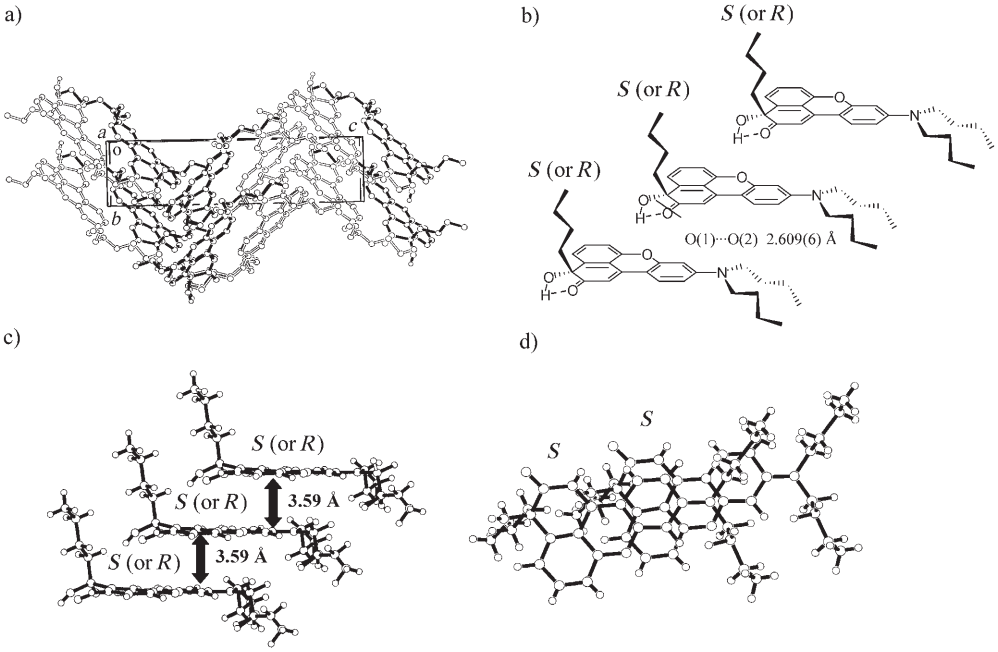

Figure 8. Crystal packing and hydrogen-bonding pattern of **5b**: a) stereoview of the molecular packing structure, b) schematic structure, c) side view, and d) top view of the overlapping of fluorophores.

drogen bonds between the hydroxyl proton and the carbonyl oxygen: (O(1)···O(2)* distances for **4a** and **4c** are 2.844(3) and 2.812(4) Å, respectively. On the other hand, in the crystal of **4b**, there are two crystallographically independent molecules. Intermolecular hydrogen bonds are also observed between the hydroxy proton and the carbonyl oxygen of each crystallographically independent molecule (O(1)···O(5) 2.81(1) and O(2)···O(4) 2.77(4) Å, respectively). Furthermore, the hydroxy proton has two proton acceptors and becomes a bifurcated-donor hydrogen to form the three-centered hydrogen bonds with the inter- and intra-molecular carbonyl oxygens. The O(1)···O(2) distances of the intramolecular hydrogen bonds are 2.767(2), 2.80(4), and 2.740(2) Å for **4a**, **4b**, and **4c** , respectively, and O(4)···O(5) in **4b** is 2.82(4) Å.

Large differences in the π-stacking of a pair of quinol enantiomers were observed among the three quinols . In the crystal of **4a**, a pair of quinol enantiomers overlap over the

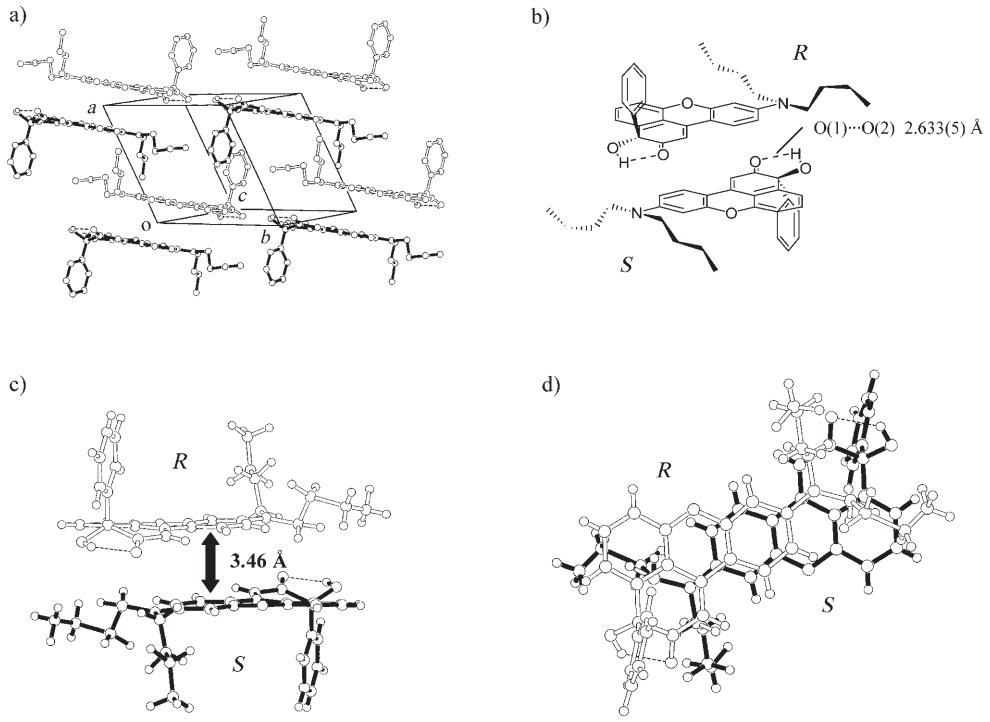

Figure 9. Crystal packing and hydrogen-bonding pattern of **5c**: a) stereoview of the molecular packing structure, b) schematic structure, c) side view, and d) top view of the pairs of fluorophores.

Table 5. Crystal data and structure refinement parameters for quinols **4a–c.**

Compound	**4a**	**4b**	**4c**
molecular formula	$C_{25}H_{29}NO_3$	$C_{56}H_{70}N_2O_6$	$C_{30}H_{31}NO_3$
formula weight	391.51	867.18	453.58
crystal size [nm]	0.45×0.40×0.60	0.20×0.20×0.70	0.30×0.20×0.50
reflns[a] (2θ range, [°])	25 (28.4–29.8)	6 (22.0–24.0)	25 (23.0–26.1)
crystal system	triclinic	monoclinic	triclinic
space group	$P\bar{1}$	Cc	$P\bar{1}$
a [Å]	9.569(2)	26.35(3)	11.081(3)
b [Å]	12.386(2)	9.6(2)	12.511(3)
c [Å]	9.418(3)	21.60(2)	10.267(2)
α [°]	93.92(2)		109.94(2)
β [°]	102.64(2)	112.54(9)	95.45(2)
γ [°]	89.10(1)		108.37(2)
V [Å^3]	1086.7(5)	5063(80)	1236.6(6)
Z	2	8	2
ρ_{calcd} [g cm^{-3}]	1.196	2.275	1.218
$F(000)$	420.00	3744.00	484.00
$\mu(Mo_{K\alpha})$ [cm^{-1}]	0.78	1.46	0.78
T [K]	296.2	296.2	296.2
scan mode	$\omega-2\theta$	$\omega-2\theta$	$\omega-2\theta$
scan rate [ω min^{-1}]	8.0[b]	8.0[b]	4.0[b]
scan width [°]	1.84 + 0.30tanθ	1.479 + 0.30tanθ	1.42 + 0.30tanθ
2θ max [°]	50.0	55.0	50.0
hkl range	−11/11, −14/14, −11/0	0/34, −12/0, −28/25	−13/13, −13/14,−12/0
reflns measured	4081	6271	4615
unique reflns	4081	5913	4348
reflns observed with $I_0>2\sigma I_0$	2497	1537	2486
R_{int}	0.015	0.031	0.294
no. of parameters	315	627	368
R	0.0679	0.0595	0.0757
Rw	0.1784	0.1326	0.1765
w	$(\sigma^2F^2)^{-1}$	$(\sigma^2F^2)^{-1}$	$(\sigma^2F^2)^{-1}$
S	2.14	1.07	1.707
max. shift/error in final cycle	0.006	2.160	0.053
max. peak in final diff. map [e Å^{-3}]	0.27	0.62	0.59
min. peak in final diff. map [e Å^{-3}]	−0.23	−0.50	-0.46

[a] Number of reflections used for unit cell determination. [b] Up to five scans.

whole molecule from the electron-donor part of benzofurano moiety containing the 9-dibutylamino group to the electron-acceptor part of naphthoquinol moiety, which is closely related to the solid-state photophysical properties. A large red shift of the absorption and fluorescence maxima and the solid-state fluorescence quenching by strong donor–acceptor-type π–π interactions of fluorescent dyes have been reported.[1f,3,5] In the crystal of **4b**, a donor–acceptor type of π-stacking between a pair of quinol enantiomers is observed; however, the rung of the π-stacking is less than that of **4a**. The distances between the benzofuranonaphthoquinol planes are approximately 3.40, 3.38, and 3.58 Å for **4a**, **4b**, and **4c**, respectively. There are seven, four, and five short interatomic π–π contacts of less than 3.6 Å in a pair of enantiomers for **4a**, **4b**, and **4c**, respectively.

Table 6. Crystal data and structure refinement parameters for quinols **5a–c**.

Compound	**5a**	**5b**	**5c**
molecular formula	$C_{25}H_{29}NO_3$	$C_{28}H_{35}NO_3$	$C_{30}H_{31}NO_3$
formula weight	391.51	433.59	453.58
crystal size [nm]	0.20×0.06×0.40	0.20×0.10×0.60	0.20×0.05×0.40
reflns[a] (2θ range, [°])	24 (22.0–24.8)	9 (22.3–23.1)	19 (22.1–24.8)
crystal system	monoclinic	monoclinic	triclinic
space group	*C*2/*c*	*P*21/*n*	$P\bar{1}$
a [Å]	33.687(4)	22.057(7)	10.026(1)
b [Å]	5.480(3)	5.578(2)	13.571(2)
c [Å]	27.233(2)	20.551(8)	9.760(2)
α [°]			97.90(1)
β [°]	120.100(6)	90.52(3)	99.66(1)
γ [°]			107.82(1)
V [Å^3]	4308(2)	2528(1)	1220.9(3)
Z	8	4	2
ρ_{calcd} [g cm^{-3}]	1.207	1.234	1.234
F(000)	1680.00	936.00	484.00
$\mu(Mo_{K\alpha})$ [cm^{-1}]	0.78	0.73	0.79
T [K]	296.2	296.2	296.2
scan mode	ω–2θ	ω–2θ	ω–2θ
scan rate [ω min^{-1}]	8.0[b]	8.0[b]	8.0[b]
scan width [°]	0.79 + 0.30 tanθ	1.47 + 0.30 tanθ	0.73 + 0.30 tanθ
2θ max [°]	50.0	55.0	50.0
hkl range	0/36, 0/6, −32/27	0/28, −7/0, −26/26	−11/11, −15/16, −11/0
reflns measured	4129	6562	4558
unique reflns	3703	5805	4558
reflns observed with $I_0 > 2\sigma I_0$	1107	1182	1752
R_{int}	0.089	0.130	0.038
no. of parameters	347	322	404
R	0.0585	0.0788	0.0715
Rw	0.1216	0.1616	0.1558
w	$(\sigma^2F^2)^{-1}$	$(\sigma^2F^2)^{-1}$	$(\sigma^2F^2)^{-1}$
S	1.10	1.13	1.30
max. shift/error in final cycle	0.002	7.557	0.036
max. peak in final diff. map [e Å^{-3}]	0.38	0.57	0.90
min. peak in final diff. map [e Å^{-3}]	−0.42	−0.48	−0.60

[a] Number of reflections used for unit cell determination. [b] Up to five scans.

In contrast, the packing structures in **5a–c** demonstrate that the quinol molecules are arranged in a "herring-bone" fashion in the crystals of **5a** and **5b**, and in a "bricks-in-a-wall" fashion in the crystal of **5c**. Intramolecular hydrogen bonding was observed between the hydroxyl proton and the carbonyl oxygen in each quinol molecule: O(1)···O(2) distances for **5a**, **5b**, and **5c** were 2.639(6), 2.609(6), and 2.633(5) Å, respectively; however, no intermolecular hydrogen bonding was observed in all three quinols. The π stacking between fluorophores is shown in Figures 7–9. The interplanar distances between the benzoxanthenone plates were about 3.59 Å for both **5a** and **5b**, and 3.46 Å for **5c**. The crystal structure of **5c** is built of centrosymmetric dimer units of enantiomers, and π stacking between a pair of enantiomers was observed over the whole molecule from the donor part of the 9-dibutylamino group to the acceptor part of the carbonyl group, which suggests strong donor–acceptor-type π–π interactions between the fluorophores. In contrast, the crystals of **5a** and **5b** show continuous π stacking of the equal enantiomers of *R* and *S* isomers to form independent columns in which there π overlapping between the naphthoquinol moiety and the 9-dibutylaminobenzo moiety of the adjacent equal enantiomers. However, a large difference in the intermolecular interactions between *R* and *S* isomers of the neighboring π-stacked columns was observed. As shown in Figure 10a, in the case of **5a**, contacts between *R* and *S* enantiomers are observed for the donor benzenering moiety that contains the 9-dibutylamino group and the carbonyl acceptor part of the naphthoquinol moiety: the shortest distance for overlapping nonbonded atoms was 3.325(8) Å. In contrast, in the case of **5b**, contacts between *R* and *S* enantiomers are observed for the acceptor parts of the naphthoquinol moieties (Figure 10b). The shortest distance for overlapping nonbonded atoms is 3.568(7) Å, so that the degree of such intermolecular interactions between fluorophores of **5b** is weak compared to that in **5a**.

From the stereostructures of **4a–c** and **5a–c**, we noticed that the substitutents affect the geometric arrangement in the crystal structure (Figure 11 and Figure 12). In **4c**, **5a**, and **5b**, the molecules are packed in the structural form with a stepped-shape because the substituent (phenyl group in **4c**, methyl group in **5a**, and butyl group in **5b**) and the 9-dibutylamino group are located on opposite sides of the molecular π plane. Therefore, the interplanar distance between the fluorophores is longer (Figure 11b and Figure 12a) so that the π–π interactions are weakened by the substituents thus leading to stronger solid-state fluorescence emission. On the other hand, in **4a**, **4b**, and **5c**, the interplanar distance between the fluorophores is short because the substituent (methyl group in **4a**, butyl group in **4b**, and phenyl group in **5c**) and the 9-dibutylamino group are located on the same side of the π plane, and the molecules are packed in a structural form with a table shape (Figure 11a and Figure 12b). The large red shift of the absorption and fluorescence maxima and the solid-state fluorescence quenching in the crystal of **5c** are considered to be induced by strong donor–acceptor-type π–π interactions.[1f,3,5] As shown above, a good correlation between the solid-state fluorescence intensity and the molecular stacking structure was observed. It was confirmed that the 5- and 3-substituents of nonconjugated linkage of **4** and **5** have a significant effect on the crystal structure. The introduction of bulky 5,5-disubstituents for the quinol **4** and 3,3-disubstituents for the quinol **5** would be

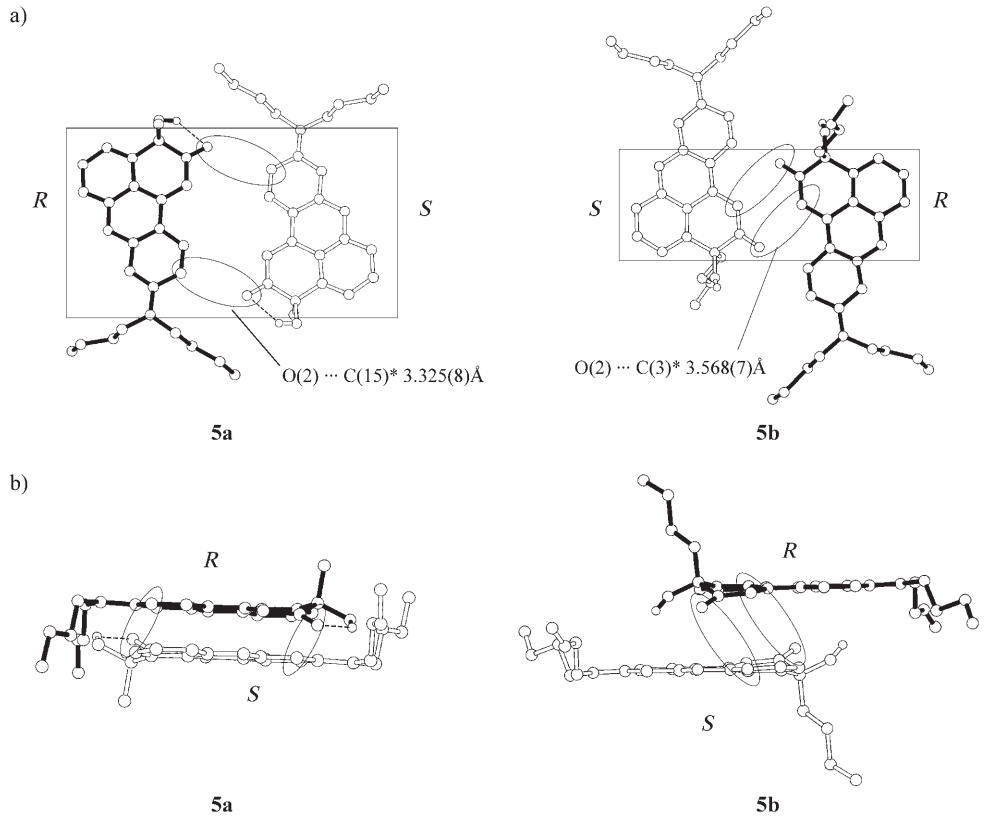

Figure 10. a) Top view and b) side view of the stacking of molecules for **5a** and **5b**.

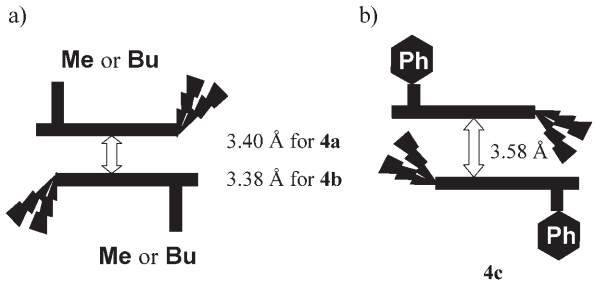

Figure 11. Schematic representation of the effects of the substituents on the interplanar distances between a pair of quinol enantiomers for a) **4a** and **4b**, and b) **4c**.

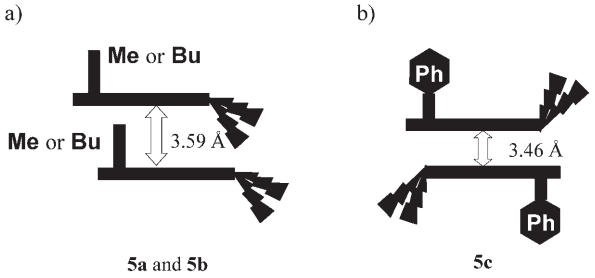

Figure 12. Schematic representation of the effects of the substituents on interplanar distances between a pair of quinols for a) **5a** and **5b**, and b) **5c**.

more effective for the improvement of the solid-state fluorescence of these fluorophores. Further studies to develop strong solid-emissive derivatives is now in progress.

Conclusion

We have synthesized novel heterocyclic quinols, 5-hydroxy-5-substituent-benzo[*b*]naphtho[1,2-*d*]furan-6-one (**4**) and 3-hydroxy-3-substituent-benzo[*kl*]xanthen-2-one (**5**) fluorophores with substituents having a nonconjugated linkage to the chromophores. The absorption and fluorescence properties of these compounds were investigated in solution and in the solid state. Dramatic substituent effects on the solid-state photophysical properties were observed and have been elucidated by means of X-ray crystallographic analyses. It was confirmed that the introduction of 5- and 3-substituents with nonconjugated linkages to the chromophores **4** and **5** can efficiently prevent short π–π contacts between the fluorophores in molecular aggregation states and thus cause a dramatic enhancement in the solid-state fluorescence.

Experimental Section

General: Melting points were measured with a Yanaco micro melting point apparatus MP-500D. IR spectra were recorded on a JASCO FT/IR-5300 spectrophotometer for samples as KBr pellets. Absorption spectra

were recorded with a JASCO U-best30 spectrophotometer, and fluorescence spectra were measured with a JASCO FP-777 spectrophotometer. Single-crystal X-ray diffraction was performed on Rigaku AFC7S diffractometer. The solid-state fluorescence excitation and emission spectra of the crystals was recorded with a JASCO FP-777 spectrometer equipped with a JASCO FP-1060 attachment. The fluorescence quantum yields (Φ) were determined by the use of 9,10-bis(phenylethynyl)anthracene (Φ = 0.84, λ_{ex} = 440 nm)[14] in benzene as the standard. Elemental analyses were recorded on a Perkin Elmer 2400 II CHN analyzer. ^{1}H NMR spectra were recorded on a JNM-LA-400 (400 MHz) FT NMR spectrometer with tetramethylsilane (TMS) as an internal standard. Column chromatography was performed on silica gel (KANTO CHEMICAL, 60 N, spherical, neutral) or alumina (WAKO, ≈300 mesh).

General synthetic procedure for 4-[(4-dibutylamino-2-hydroxy)phenyl]-[1,2]naphthoquinone (1): *m*-(Dibutylamino)phenol (1.28 g, 5.67 mmol) was added to a solution of sodium 1,2-naphthoquinone-4-sulfonate (1.00 g, 3.84 mmol) and $NiCl_2$(0.50 g, 3.84 mmol) in DMF (25 mL) with stirring at 50 °C. After further stirring for 2 h, the reaction mixture was poured into water. The resulting precipitate was filtered, washed with water, and dried. The residue was chromatographed (silica gel, CH_2Cl_2/ethyl acetate 20:1) to give **1** (0.54 g, yield 37 %) as a blue powder. M.p. 142–144 °C; ^{1}H NMR (400 MHz, [D$_6$]acetone, TMS): δ = 0.98 (t, 6H), 1.35–1.45 (m, 4H), 1.60–1.68 (m, 4H), 3.37 (t, 4H), 6.35 (s, 1H, -OH), 6.36 (d, J = 2.44 Hz, 1H), 6.39 (dd, J = 2.44 and 8.56 Hz, 1H), 7.11 (d, J = 8.56 Hz, 1H), 7.42 (dd, J = 1.48 and 7.56 Hz, 1H), 7.57 (td, J = 1.48 and 7.56 Hz, 1H), 7.65 (td, J = 1.48 and 7.56 Hz, 1H), 8.04 (dd, J = 1.48 and 7.56 Hz, 1H), 8.34 ppm (s, 1H); IR (KBr): $\tilde{\nu}$ = 3374, 1605 cm^{-1}; UV/Vis (1,4-dioxane): λ_{max} (ε) = 507 (4700), 394 nm (3900 mol^{-1}m^{3}cm^{-1}); elemental analysis calcd (%) for $C_{24}H_{27}NO_3$: C 76.36, H 7.21, N 12.72; found: C 76.06, H 7.01, N 12.54.

General synthetic procedure for 9-dibutylamino-benzo[*b*]naphtho[1,2-*d*]furan-5,6-dione (2): *m*-(Bibutylamino)phenol (1.28 g, 5.67 mmol) was added to a solution of sodium 1,2-naphthoquinone-4-sulfonate (1.00 g, 3.84 mmol) and $NiCl_2$ (0.50 g, 3.84 mmol) in acetic acid (25 mL) with stirring at 50 °C. After further stirring for 1 h, the solvent was evaporated and the residue was extracted with CH_2Cl_2. The organic extract was washed with water. The CH_2Cl_2 extract was evaporated, and the residue was chromatographed (silica gel, CH_2Cl_2/ethyl acetate 10:1) to give **2** (0.55 g, yield 38 %) as a green powder. M.p. 149–153 °C; ^{1}H NMR (400 MHz, [D$_3$]chloroform, TMS): δ = 1.00 (t, 6H), 1.37–1.50 (m, 4H), 1.62–1.74 (m, 4H), 3.34 (t, 4H), 6.44 (d, J = 2.20 Hz, 1H), 6.74 (dd, J = 2.2 and 9.02 Hz, 1H), 7.36 (td, J = 1.24 and 7.56 Hz, 1H), 7.57 (td, J = 1.48 and 7.56 Hz, 1H), 7.71 (d, J = 9.02 Hz, 1H), 7.78 (dd, J = 1.48 and 7.56 Hz, 1H), 7.96 ppm (dd, J = 1.24 and 7.56 Hz, 1H); IR (KBr): $\tilde{\nu}$ = 1645 cm^{-1}; UV/Vis (1,4-dioxane): λ_{max} (ε) = 542 (11400), 406 nm (9000 mol^{-1}m^{3}cm^{-1}); elemental analysis calcd (%) for $C_{24}H_{25}NO_3$: C 76.77, H 6.71, N 3.73; found: C 76.91, H 6.83, N 3.76.

General synthetic procedure for 9-(dibutylamino)benzo[*kl*]xanthene-2,3-dione (3): A solution of quinone **1** (1.45 g, 3.84 mmol) and [Cu(OCOCH$_3$)$_2$] (0.70 g, 3.84 mmol) in DMSO (25 mL) was stirred at 100 °C for 7 h. After the reaction was complete, the mixture was poured into water. The resulting precipitate was filtered, washed with water, and dried. The residue was chromatographed (silica gel, CH_2Cl_2/ethyl acetate 10:1) to give **2**[5] (0.22 g, yield 15 %) as a green powder and **3** (0.95 g, yield 66 %) as a purple powder.

Compound ***3***: M.p. 132–134 °C; ^{1}H NMR (400 MHz, [D$_6$]acetone, TMS): δ = 1.00 (t, 6H), 1.40–1.50 (m, 4H), 1.65–1.73 (m, 4H), 3.52 (t, 4H), 6.50 (d, J = 2.68 Hz, 1H), 6.55 (s, 1H), 6.87 (m, 1H), 7.60 (m, 1H), 7.71 (m, 1H), 7.89–7.91 ppm (m, 2H); IR (KBr): $\tilde{\nu}$ = 1594 cm^{-1}; UV/Vis (1,4-dioxane): λ_{max} (ε) = 530 (16000), 436 (10100), 346 nm (7000 mol^{-1}m^{3}cm^{-1}); elemental analysis calcd (%) for $C_{24}H_{25}NO_3$: C 76.77, H 6.71, N 3.73; found: C 76.88, H 6.90, N 3.59.

General synthetic procedure for quinols 4a–c and 5a–c by the reaction of quinone 2 or 3 with organolithium reagents: An ethereal solution of organolithium (RLi: MeLi, BuLi, and PhLi) at −108 °C was added over 15 min to a solution of quinone **2** (or **3**) in THF (200 mL) under an Ar atmosphere. During the course of addition, the red solution turned to a reddish brown solution. After the mixture had been stirred for 15 min at room temperature, the reaction was quenched with saturated NH_4Cl solution. The solvent was evaporated, and the residue was extracted with CH_2Cl_2. The organic extract was washed with water. The CH_2Cl_2 extract was evaporated, and the residue was chromatographed (silica gel, CH_2Cl_2/AcOEt 3:1) to give **2** (or **3**) and **4** (or **5**). The product yields of **4** and **5**, and the recovered yields of **2** and **3** are shown in Table 2.

9-Dibutylamino-5-hydroxy-5-methyl-5*H*-benzo[*b*]naphtho[1,2-*d*]furan-6-one (4a): Yield: 67 %; m.p. 151–152 °C; ^{1}H NMR (400 MHz, [D$_3$]chloroform, TMS): δ = 0.99 (t, 6H), 1.35–1.45 (m, 4H), 1.60–1.67 (m, 7H), 3.38 (t, 4H), 3.71 (s, 1H, -OH), 6.73 (d, J = 1.96 Hz, 1H), 6.83 (dd, J = 1.96 and 9.04 Hz, 1H), 7.41–7.48 (m, 2H), 7.78–7.83 (m, 1H), 7.96 (d, J = 9.04 Hz, 1H), 8.01–8.06 ppm (m, 1H); IR (KBr): $\tilde{\nu}$ = 3432, 1644 cm^{-1}; elemental analysis calcd (%) for $C_{25}H_{29}NO_3$: C 76.70, H 7.47, N 3.58; found: C 76.70, H 7.52, N 3.54.

9-Dibutylamino-5-hydroxy-5-butyl-5*H*-benzo[*b*]naphtho[1,2-*d*]furan-6-one (4b): Yield: 47 %; m.p. 113–115 °C; ^{1}H NMR(400 MHz, [D$_6$]acetone, TMS): δ = 0.73 (t, 3H), 0.99 (t, 6H), 1.10–1.99 (m, 14H), 3.50 (t, 4H), 4.68 (s, 1H), 6.82 (d, J = 2.20 Hz, 1H), 6.99 (dd, J = 2.20 and 9.03 Hz, 1H), 7.44–7.50 (m, 2H), 7.75–7.79 (m, 1H), 8.14–8.19 ppm (m, 2H); IR (KBr): $\tilde{\nu}$ = 3409, 1614 cm^{-1}; elemental analysis calcd (%) for $C_{28}H_{35}NO_3$: C 77.56, H 8.14, N 3.23; found: C 77.36, H 8.32, N 3.22.

9-Dibutylamino-5-hydroxy-5-phenyl-5*H*-benzo[*b*]naphtho[1,2-*d*]furan-6-one (4c): Yield: 30 %; m.p. 164–168 °C; ^{1}H NMR(400 MHz, [D$_3$]chloroform, TMS): δ = 0.98 (t, 6H), 1.25–1.67 (m, 8H), 3.38 (t, 4H), 4.53 (s, 1H, -OH), 6.69 (d, J = 2.2, 1H), 6.85 (dd, J = 2.2 and 9.28 Hz, 1H), 7.17–7.26 (m, 3H), 7.34–7.38 (m, 2H), 7.39–7.48 (m, 2H), 7.62 (dd, J = 1.22 and 7.8 Hz, 1H), 8.01 (d, J = 9.28 Hz, 1H), 8.09 ppm (d, J = 7.8 Hz, 1H); IR (KBr): $\tilde{\nu}$ = 3449, 1652 cm^{-1}; elemental analysis calcd (%) for $C_{30}H_{31}NO_3$: C 79.44, H 6.89, N 3.09; found: C 79.48, H, 6.96, N 2.96.

9-Dibutylamino-3-hydroxy-3-methyl-3*H*-benzo[*kl*]xanthen-2-one (5a): Yield: 49 %; m.p. 113–115 °C; ^{1}H NMR(400 MHz, [D$_6$]acetone, TMS): δ = 0.99 (t, 6H), 1.39–1.47 (m, 7H), 1.63–1.71 (m, 4H), 3.49 (t, 4H), 4.48 (s, 1H), 6.24 (s, 1H), 6.51 (d, J = 2.44 Hz, 1H), 6.82 (dd, J = 2.44 and 9.28 Hz, 1H), 7.23 (dd, J = 1.20 and 7.56 Hz, 1H), 7.49 (dd, J = 1.20 and 7.56 Hz, 1H), 7.57 (d, J = 7.56 Hz, 1H), 7.87 ppm (d, J = 9.28 Hz, 1H); IR (KBr): $\tilde{\nu}$ = 3433, 1643 cm^{-1}; elemental analysis calcd (%) for $C_{25}H_{29}NO_3$: C 76.70, H 7.47, N 3.58; found: C 76.55, H 7.62, N 3.59.

9-Dibutylamino-3-hydroxy-3-butyl-3*H*-benzo[*kl*]xanthen-2-one (5b): Yield: 37 %; m.p. 130–132 °C; ^{1}H NMR(400 MHz, [D$_6$]acetone, TMS): δ = 0.77 (t, 3H), 0.99 (t, 6H), 1.09–1.80 (m, 14H), 3.50 (t, 4H), 4.44 (s, 1H), 6.24 (d, J = 2.44, 1H), 6.51 (dd, J = 2.44 and 9.28 Hz, 1H), 6.83 (dd, J = 2.44 and 9.27 Hz, 1H), 7.23 (dd, J = 1.20 and 8.04 Hz, 1H), 7.51 (dd, J = 1.20 and 7.56 Hz, 1H), 7.57–7.59 (m, 1H), 7.87 ppm (d, J = 9.28 Hz, 1H); IR (KBr): $\tilde{\nu}$ = 3445, 1601 cm^{-1}; elemental analysis calcd (%) for $C_{28}H_{35}NO_3$: C 77.56, H 8.14, N 3.23; found: C 77.35, H 8.39, N 3.38.

9-Dibutylamino-3-hydroxy-3-phenyl-3*H*-benzo[*kl*]xanthen-2-one (5c): Yield: 17 %; m.p. 174–176 °C; ^{1}H NMR(400 MHz, [D$_6$]acetone, TMS): δ = 0.99 (t, 6H), 1.40–1.73 (m, 8H), 3.52 (t, 3H), 5.53 (s, 1H), 6.24 (s, 1H), 6.55 (d, J = 2.44, 1H), 6.85 (dd, J = 2.44 and 9.28 Hz, 1H), 7.15–7.43 (m, 7H), 7.57 (m, 1H), 7.89 ppm (d, J = 9.28 Hz, 1H); IR (KBr): $\tilde{\nu}$ = 3440, 1639 cm^{-1}; elemental analysis calcd (%) for $C_{30}H_{31}NO_3$: C 79.44, H 6.89, N 3.09; found: C 79.26, H 6.99, N 3.11.

X-ray crystallographic studies: The reflection data were collected at 23 ± 1 °C on a Rigaku AFC7S four-circle diffractometer by a 2θ–ω scan technique with graphite-monochromated Mo$_{K\alpha}$ (λ = 0.71069 Å) radiation at 50 kV and 30 mA. In all case, the data were corrected for Lorentz and polarization effects. A correction for secondary extinction was applied. The reflection intensities were monitored by three standard reflections for every 150 reflections. An empirical absorption correction based on azimuthal scans of several reflections was applied. All calculations were performed with the teXsan[15] crystallographic software package of Molecular Structure Corporation. CCDC-294660 (**4a**), CCDC-294661 (**4b**), CCDC-294662 (**4c**) CCDC-294192 (**5a**), CCDC-294193 (**5b**), and CCDC-294194 (**5c**) contain the supplementary crystallographic data (see Tables 5) for this paper. These data can be obtained free of charge via www.ccdc.cam.ac.uk/data_request/cif.

*Compound **4a***: Crystals of **4a** were obtained as air-stable, orange prisms by recrystallization from dichloromethane/*n*-hexane. The transmission factors ranged from 0.98 to 1.00. The crystal structure was solved by direct methods with SIR88.[16] The structures were expanded with Fourier techniques.[17] The non-hydrogen atoms were refined anisotropically. Some hydrogen atoms were refined isotropically, the rest were fixed geometrically and not refined.

*Compound **4b***: Crystals of **4b** were obtained as air-stable, green prisms by recrystallization from dichloromethane/*n*-hexane. The transmission factors ranged from 0.82 to 1.00. The crystal structure was solved by direct methods with SIR92.[18] The structures were expanded with Fourier techniques.[17] The non-hydrogen atoms were refined anisotropically. Some hydrogen atoms were refined isotropically, the rest were fixed geometrically and not refined.

*Compound **4c***: Crystals of **4c** were obtained as air-stable, yellow-orange prisms by recrystallization from dichloromethane/*n*-hexane. The transmission factors ranged from 0.96 to 1.00. The crystal structure was solved by direct methods with SIR88.[16] The structures were expanded with Fourier techniques.[17] The non-hydrogen atoms were refined anisotropically. Some hydrogen atoms were refined isotropically, the rest were fixed geometrically and not refined.

*Compound **5a***: Crystals of **5a** were obtained as air-stable orange prisms by recrystallization from dichloromethane/*n*-hexane. The transmission factors ranged from 0.94 to 1.00. The crystal structure was solved by direct methods using SIR92.[18] The structures were expanded using Fourier techniques.[17] The non-hydrogen atoms were refined anisotropically. Some hydrogen atoms were refined isotropically, the rest were fixed geometrically and not refined.

*Compound **5b***: Crystals of **5b** were obtained as air-stable orange prisms by recrystallization from acetonitrile. The transmission factors ranged from 0.54 to 1.00. The crystal structure was solved by direct methods with SAPI91.[19] The structures were expanded using Fourier techniques.[17] The non-hydrogen atoms were refined anisotropically. Some hydrogen atoms were refined isotropically, the rest were fixed geometrically and not refined.

*Compound **5c***: Crystals of **5c** were obtained as air-stable orange prisms by recrystallization from dichloromethane/*n*-hexane. The transmission factors ranged from 0.95 to 1.00. The crystal structure was solved by direct methods with SIR92.[18] The structures were expanded using Fourier techniques.[17] The non-hydrogen atoms were refined anisotropically. Some hydrogen atoms were refined isotropically, the rest were fixed geometrically and not refined.

Acknowledgements

This work was partially supported by the Regional Science Promotion (RSP) program of Japan Science and Technology of Agency (JST) and by a Special Research Grant for Green Science from Kochi University. Y.O. was supported by research fellowships from the Japan Society for the Promotion of Science (JSPS) for young scientists.

[1] a) K. Hirano, S. Minakata, M. Komatsu, *Chem. Lett.* **2001**, 8; b) Y. Sonoda, Y. Kawanishi, T. Ikeda, M. Goto, S. Hayashi, N. Tanigaki, K. Yase, *J. Phys. Chem. B* **2003**, *107*, 3376; c) R. Davis, S. Abraham, N. P. Rath, S. Das, *New J. Chem.* **2004**, *28*, 1368; d) V. de Halleux, J.-P. Calbert, P. Brocorens, J. Cornil, J.-P. Declercq, J.-L. Brédas, Y. Geerts, *Adv. Funct. Mater.* **2004**, *14*, 649; e) H.-C. Yeh, W.-C. Wu, Y.-S. Wen, D.-C. Dai, J.-K. Wang, C.-T. Chen, *J. Org. Chem.* **2004**, *69*, 6455; f) E. Horiguchi, S. Matsumoto, K. Funabiki, M. Matsui, *Bull. Chem. Soc. Jpn.* **2005**, *78*, 1167; g) S. Mizukami, H. Houjou, K. Sugaya, E. Koyama, H. Tokuhisa, T. Sasaki, M. Kanesato, *Chem. Mater.* **2005**, *17*, 50; h) Y. Mizobe, N. Tohnai, M. Miyata, Y. Hasegawa, *Chem. Commun.* **2005**, 1839; i) I. Vayá, M. C. Jiménez, M. Miranda, *Tetrahedron: Asymmetry* **2005**, *16*, 2167; j) Z. Xie, B. Yang, L. Liu, M. Li, D. Lin, Y. Ma, G. Cheng, S. Liu, *J. Phys. Org. Chem.* **2005**, *18*, 962.

[2] a) C. W. Tang, S. A. VansSlyke, *Appl. Phys. Lett.* **1987**, *51*, 913; b) C. W. Tang, S. A. VansSlyke, C. H. Chen, *J. Appl. Phys.* **1989**, *65*, 3610; c) J. Schi, C. W. Tang, *Appl. Phys. Lett.* **1997**, *70*, 1665; d) A. Kraft, A. C. Grimsdale, A. B. Holmes, *Angew. Chem.* **1998**, *110*, 416–443; *Angew. Chem. Int. Ed.* **1998**, *37*, 402; e) U. Mitschke, P. Bäuerle, *J. Mater. Chem.* **2000**, *10*, 1471; f) K.-C. Wong, Y. -Y. Chien, R.-T. Chen, C.-F. Wang, Y.-T. Liu, H.-H. Chiang, P.-Y. Hsieh, C.-C. Wu, C. H. Chou, Y. O. Su, G.-H. Lee, S.-M. Peng, *J. Am. Chem. Soc.* **2002**, *124*, 11576; g) C. J. Tonzola, M. M. Alam, W. K. Kaminsky, S. A. Jenekhe, *J. Am. Chem. Soc.* **2003**, *125*, 13548; h) H.-C. Yeh, L.-H. Chan, W.-C. Wu, C.-T. Chen, *J. Mater. Chem.* **2004**, *14*, 1293; i) C.-T. Chen, *Chem. Mater.* **2004**, *16*, 4389; j) C.-L. Chiang, M.-F. Wu, D.-C. Dai, Y.-S. Wen, J.-K. Wang, C.-T. Chen, *Adv. Funct. Mater.* **2005**, *15*, 231.

[3] a) K. Yoshida, Y. Ooyama, H. Miyazaki, S. Watanabe, *J. Chem. Soc. Perkin Trans. 2* **2002**, 700–707; b) Y. Ooyama, T. Nakamura, K. Yoshida, *New J. Chem.* **2005**, *29*, 447.

[4] a) Z. Fei, N. Kocher, C. J. Mohrschladt, H. Ihmels, D. Stalke, *Angew. Chem.* **2003**, *115*, 807–811; *Angew. Chem. Int. Ed.* **2003**, *42*, 783; b) J. L. Scott, T. Yamada, K. Tanaka, *New J. Chem.* **2004**, *28*, 447.

[5] a) K. Yoshida, J. Yamazaki, Y. Tagashira, S. Watanabe, *Chem. Lett.* **1996**, 9; b) K. Yoshida, T. Tachikawa, J. Yamasaki, S. Watanabe, S. Tokita, *Chem. Lett.* **1996**, 1027; c) K. Yoshida, H. Miyazaki, Y. Miura, Y. Ooyama, S. Watanabe, *Chem. Lett.* **1999**, 837; d) K. Yoshida, Y. Ooyama, S. Tanikawa, S. Watanabe, *Chem. Lett.* **2000**, 714; e) K. Yoshida, Y. Ooyama, S. Tanikawa, S. Watanabe, *J. Chem. Soc. Perkin Trans. 2* **2002**, 708–714; f) Y. Ooyama, K. Yoshida, *New J. Chem.* **2005**, *29*, 1204.

[6] K. Yoshida, K. Uwada, H. Kumaoka, L. Bu, S. Watanabe, *Chem. Lett.* **2001**, 808.

[7] H. Langhals, T. Potrawa, H. Nöth, G. Linti, *Angew. Chem.* **1989**, *101*, 497–499; *Angew. Chem. Int. Ed. Engl.* **1989**, *28*, 478–480.

[8] A. Dreuw, J. Plötner, L. Lorenz, J. Wachtveitl, J. E. Djanhan, J. Brüning, T. Metz, M. Bolte, M. U. Schmidt, *Angew. Chem.* **2005**, *117*, 7961–7964; *Angew. Chem. Int. Ed.* **2005**, *44*, 7783–7786.

[9] K. Yoshida, N. Oga, T. Koujiri, M. Ishiguro, Y. Kubo, *J. Chem. Soc. Perkin Trans. 1* **1990**, 189.

[10] a) A. Fischer, G. N. Henderson, *Tetrahedron Lett.* **1980**, *21*, 701; b) A. Fischer, G. N. Henderson, *Tetrahedron Lett.* **1983**, *24*, 131; c) J. Mckinley, A. Aponick, J. C. Raber, C. Fritz, D. Montgomery, C. T. Wigal, *J. Org. Chem.* **1997**, *62*, 4874.

[11] K. Kalyanasundaram, J. K. Thomas, *J. Phys. Chem.* **1977**, *81*, 2176.

[12] B. Valeur, *Molecular Fluorescence*, Wiley-VCH, Weinheim, **2002**.

[13] T. Yoshihara, H. Shimada, H. Shizuka, S. Tobita, *Phys. Chem. Chem. Phys.* **2001**, *3*, 4972.

[14] C. A. Heller, R. A. Henry, B. A. Mclaughlin, D. E. Bills, *J. Chem. Eng. Data* **1974**, *19*, 214.

[15] teXsan: Crystal Structure Analysis Package, Molecular Structure Corporation **1985** and **1992**.

[16] M. C. Burla, M. Camalli, G. Cascaeano, C. Giacovazzo, G. Polidori, R. Spagna, D. Viterbo, *J. Appl. Crystallogr.* **1989**, *22*, 389.

[17] DIRDIF94. P. T. Beurskens, G. Admiraal, G. Beurskens, W. P. Bosman, R. de Gelder, R. Israel, J. M. M. Smits, The DIRIF94 program system, Technical Report of the Crystallography Laboratory, University of Nijmegen, The Netherlands, **1994**.

[18] A. Altomare, M. C. Burla, M. Camalli, M. Cascarano, C. Giacovazzo, A. Guagliardi, G. Polidori, *J. Appl. Crystallogr.* **1994**, *27*, 435.

[19] Hai-Fu Fan, Structure Analysis Programs with Intelligent Control, Rigaku Corporation, Tokyo, Japan, **1991**.

Received: January 21, 2006
Revised: April 9, 2006
Published online: July 13, 2006

